Multi-omics approach to identify bacterial polyynes and unveil their antifungal mechanism against *Candida albicans*

Ching-Chih Lin[1#], Sin Yong Hoo[1#], Chih Lin[1], Kai-Fa Huang[2], Ying-Ning Ho[3], Chi-Hui Sun[1], Han-Jung Lee[1], Pi-Yu Chen[1], Lin-Jie Shu[1], Bo-Wei Wang[1], Wei-Chen Hsu[1], and Yu-Liang Yang[1]*

[1]Agricultural Biotechnology Research Center, Academia Sinica, Taipei 11529, Taiwan

[2]Institute of Biological Chemistry, Academia Sinica, Taipei 11529, Taiwan

[3]Institute of Marine Biology and Center of Excellence for the Oceans, National Taiwan Ocean University, Keelung 20224, Taiwan

[#]These authors contributed equally to this work.

*Corresponding author: Dr. Yu-Liang Yang

Phone number: +886-2-2787-2089

E-mail: ylyang@gate.sinica.edu.tw

Abstract

Bacterial polyynes are highly active natural products with a broad-spectrum of antimicrobial activities. However, their detailed mechanism of action remains unclear. Through integrating comparative genomics, transcriptomics, functional genetics, and metabolomics analysis, we identified a unique polyyne resistance gene, *masL* (encoding acetyl-CoA acetyltransferase), from the biosynthesis gene cluster (BGC) dominant for the production of antifungal polyynes (massilin A, massilin B, collimonin C, and collimonin D) in *Massilia* sp. YMA4. Phylogenic and chemotaxonomic analyses characterized the core architecture of bacterial polyyne BGC. The crystallographic analysis of the MasL-collimonin C complex indicated that bacterial polyynes serve as a covalent inhibitor of acetyl-CoA acetyltransferase. Moreover, we confirmed that the bacterial polyynes disrupted cell membrane integrity and inhibited cell viability of *Candida albicans* by targeting ERG10 (homolog of MasL). Overall, understanding of the antifungal mechanism of bacterial polyynes presented herein will be useful for the development of polyynes for fungal infections.

Introduction

Invasive fungal infections caused by *Candida*, *Aspergillus*, *Pneumocystis*, and *Cryptococcus* spp. in humans result in approximately 1.4 million deaths per year worldwide[1]. *Candida albicans* is the most prevalent pathogen among the *Candida* spp., causing an invasive fungal infection called Invasive Candidiasis (IC)[2]. The clinical guidelines for the management of Candidiasis offered by the Infectious Diseases Society of America recommend echinocandin and azole-type drugs as initial therapy for Candidiasis[3]. Echinocandin inhibits fungal cell wall synthesis by targeting 1,3-β-glucan synthase and the azoles interfere with fungal cell membrane formation by inhibiting lanosterol 14α-demethylase[4, 5]. However, more and more azole-resistant *Candida* spp. are being isolated from hospital IC patients due to drug abuse of azoles[6]. Because of the increasing severity of drug resistance and the limited number of clinical drugs currently available for treatment, new types of antifungal agents are urgently required[5, 7].

Polyynes or polyacetylenes, a substantial class of compounds derived from polyunsaturated fatty acids, contain a conformationally rigid rod-like architecture and an electron-rich consecutive acetylene moiety. Hundreds of polyynes have been discovered, out of which compounds have mostly been isolated from terrestrial plants such as (*3R*)-falcarinol and ichthyothereol[8]. In contrast to polyynes from plant sources, bacterial polyynes contain a distinguished terminal alkyne with conjugated systems, which causes bacterial polyynes to be more unstable. This instability has discouraged surveys of bacterial polyynes using the bioactivity-guided isolation approach. To date, only 12 bacterial polyynes have been recorded in a few species. However, these polyynes have been reported to have a broad spectrum of antimicrobial effects. For instance, cepacin, isolated from *Pseudomonas cepacia* (taxonomically reclassified as a *Burkholderia diffusa*), was reported to have anti-bacterial activity against the majority Gram-negative bacteria, staphylococci, and anti-oomycetal activity against *Pythium ultimum*[9, 10]; collimonins isolated from *Collimonas fungivorans* Ter331[11, 12] and Sch 31828 isolated from *Microbispora* sp. SCC1438[13] were reported to have antifungal activity against *Aspergillus niger* and *Candida* spp., respectively. Despite the apparent antibiotic effect of these compounds, the active target and mechanism(s) remain unclear.

Here, we delineated the antifungal mechanism of bacterial polyynes. We used a multi-omic approach to identify the bioactive polyynes of *Massilia* sp. YMA4 and

characterized their biosynthesis gene cluster (BGC). By comparing bacterial polyyne BGCs via genome mining, we revealed that bacterial polyynes are antifungal agents that act by targeting the first enzyme of ergosterol biosynthesis, acetyl-CoA acetyltransferase. Crystallographic analysis unveiled the detailed binding model of polyynes to the acetyl-CoA acetyltransferase. This information will be useful in new antifungal drug screening and ligand-based drug design.

Results

Transcriptomics analysis reveals polyynes as antifungal agents and their encoding BGC in *Massilia* sp. YMA4

Based on a previous survey, *Massilia* sp. YMA4 has antimicrobial effects against *Staphylococcus aureus*, *Staphylococcus epidermidis*, *Paenibacillus larvae*, and the pathogenic fungus, *C. albicans*[14]. In antagonism assay of *Massilia* sp. YMA4 against *C. albicans,* a distinct phenotype showed that the antifungal agent was produced in potato dextrose agar (PDA) medium but not in yeast malt agar (YMA) medium (**Fig. 1a**) and this was further confirmed by disc diffusion assay. Notably, we found that the antifungal metabolites were unstable in the extract and hard to scale up for bioassay using the classic bioactivity-guided isolation approach. Therefore, to mine the antifungal metabolites, a combined transcriptomics and metabolomics approach was used to identify the compounds produced in the two different media (PDA and YMA). First, the circular genome of *Massilia* sp. YMA4 was assembled as 6.33 megabase pairs (Mbp) with 5315 coding sequences (CDSs) by the PacBio sequencing system (**Fig. 1b**). Then transcriptomics analysis of *Massilia* sp. YMA4 cultured in the two media, processed using the Illumina platform was conducted. It showed differential expression with 192 upregulated genes and 226 downregulated genes in PDA compared to YMA (with $P < 0.05$ and |fold-change| > 2, **Supplementary Fig. 1a and Data 1**). Then, we assigned these 418 differentially expressed genes (DEGs) into 77 pathways for pathway analysis using the Kyoto Encyclopedia of Genes and Genomes (KEGG)[15]. The results identified a total of eight significantly enriched pathways involved in different culture conditions (FDR-adjusted $P < 0.05$, **Supplementary Fig. 1b and Data 2**). Compared to YMA, the enriched pathways in PDA were conspicuously associated with small-molecule metabolism, especially fatty acid-related metabolism.

108 To mine the biosynthesis genes encoding the unstable antifungal metabolites,
109 an *in-silico* BGC identification combined the results of rule-based antiSMASH
110 (bacterial version, v.5)[16] and deep learning annotation DeepBGC[17] to characterize
111 19 BGCs in *Massilia* sp. YMA4 (annotation list shown in **Supplementary Data 3**).
112 Combining the BGC mining and transcriptomics results, we found that the predicted
113 gene cluster 17 is the only BGC highly and consistently expressed with most genes
114 in PDA compared to YMA. We named the predicted gene cluster 17 as massilin
115 (*mas*) BGC with 12 transcribed genes (*masA* to *masL*). The unique features of *mas*
116 BGC are genes encoding fatty acyl-AMP ligase (*masD*) and acyl carrier protein
117 (*masG*) for fatty acid substrate loading, and modification encoding genes fatty acid
118 desaturases (*masA*, *masE*, *masF* and *masH*) and hydrolases (*masI* and *masK*)
119 (**Supplementary Table 1**).
120
121 **Characterization of *mas* BGC producing polyynes by *Massilia* sp. YMA4**
122 To identify the metabolites of *mas* BGC, we constructed a biosynthesis-deficient
123 mutant strain (Δ*masH*) through insertion mutation at the *masH* gene locus in *Massilia*
124 sp. YMA4. Δ*masH* lost antifungal activity against type strain ATCC18804 of *C.*
125 *albicans* and clinically isolated fluconazole-resistant *C. albicans* and *C.tropicali*
126 (**Supplementary Fig. 2**). Next, we conducted target isolation using the differential
127 features identified in the UPLC-DAD-HRMS/MS analysis of wild-type and Δ*masH*
128 (**Supplementary Fig. 3**). Then, we purified four major polyynes from ethyl acetate
129 extract. Their structures were elucidated by high-resolution mass spectrometry
130 (**Supplementary Fig. 3 and 4**) and nuclear magnetic resonance (NMR). Of the four,
131 collimonin C **1** and collimonin D **2** were reported in a previous study isolated from *C.*
132 *fungivorans* Ter331[11]. A new compound with an ene-triyne moiety was named
133 massilin A **3**, which was identified as a racemate with a hydroxyl group at the C6
134 position of the unsaturated hexadecanoic acid backbone. Another new compound
135 with an ene-diyne-ene moiety named massilin B **4** was supposed to be the precursor
136 of collimonin C **1** or collimonin D **2**. Notably, massilin B **4** is more chemically stable
137 than other polyynes with a terminal alkyne. The four polyynes were biosynthesized
138 by a *mas* BGC putatively derived from palmitic acid with multiple cycles of
139 desaturation and oxidation modification.
140 For antifungal activity assay, polyynes with a terminal alkyne moiety showed
141 potent inhibition of *C. albicans* with minimum inhibitory concentrations (MIC): 69.73

142 μM (collimonin C **1**), 35.24 μM (collimonin D **2**) and 2.40 μM (massilin A **3**). However,
143 massilin B **4** with a terminal alkene moiety had no antifungal activity with MIC > 500
144 μM (**Table 1** and **Supplementary Fig. 5**). These results imply that the terminal
145 alkyne is an essential functional moiety for the antifungal activity of the polyynes.
146

147 **Phylogenetic analysis of polyyne BGCs and their genetic-chemotaxonomy**
148 **relationship**

149 A phylogenetic analysis was performed on *mas* BGC and its homologous BGCs
150 from finished sequenced bacterial genomes. We used fully transcribed genes of *mas*
151 BGC as a template to process multiple sequence alignments for mining the polyyne
152 BGCs by using MultiGeneBlast[18] in the bacterial genome database (BCT, 2020
153 November, NCBI) and additional genomes of polyyne producing bacteria
154 (**Supplementary Data 4**). The results revealed that polyyne BGCs were
155 discontinued in bacterial phylogeny and appeared in certain genera in bacteria.
156 Among the homologous polyyne BGCs in 56 bacteria genomes, we recognized a
157 consensus region of polyyne BGC with a unique gene cluster architecture: fatty acyl-
158 AMP ligase (FAAL) - 2x fatty acid desaturase (FAD) - acyl carrier protein (ACP) -
159 fatty acid desaturase (FAD) – hydrolases/thioesterase (H/TE).

160 In view of the conservation of the gene cluster architecture, the concatenated
161 amino acid sequence of the consensus region was used to build a phylogenetic tree,
162 and the bacterial species could be intergraded into 11 leaves (**Fig. 2a** and
163 **Supplementary Data 5**). Based on the reported polyyne structures (**Fig. 2b**), we
164 configured polyyne BGCs into three monophyla: the palmitate-derived polyynes
165 family (**C16**) containing the *Massilia* group (this study, compounds **1**-**4**), the
166 *Collimonas* group (*C. fungivorans* Ter331, compounds **1**, **2**, **7** and **8**[11]) and the
167 *Burkholderia* group 2 (*B. ambifaria* BCC019, compounds **5** and **6**[9]) with an outgroup
168 of *Streptomyces* group and *Amycolatopsis orientalis*; the Stearate-derived polyynes
169 family (**C18**) contains the *Trinickia* group (*T. caryophylli*, compound **9**[19, 20]),
170 *Burkholderia* group 1 (*B. gladioli* BSR3, compound **9**[20]), *Pseudomonas* group (*P.*
171 *protegens* Cab57, compounds **10** and **11**[21]) and *Gynuella sunshinyii* (ergoynes A,
172 polyyne derivate[22]); and the uncharacterized monophylum with *Mycobacterium*
173 group and *Nocardia brasiliensis*. The phylogenic and chemotaxonomy relationship
174 suggests that polyyne BGCs might first have evolved with an adaptive mutation for a
175 different substrate-specific family before spreading within the family.

176

177 **MasL serves as a polyyne direct target and has a protective function**

178 We further analyzed the palmitate-derived polyyne (**C16**) monophylum, including
179 *mas* BGC in *Massilia* sp. YMA4 (**Fig. 2c-i**), *ccn* BGC in *B. ambifaria* BCC019 [9](**Fig.**
180 **2c-ii**), and *col* BGC in *C. fungivorans* Ter331[12](**Fig. 2c-iii**). The phylogenetic
181 analysis showed that *ccn* BGC branched out before the most recent common
182 ancestor of *mas/col* BGCs, which implies that *ccn* BGC is the evolutionary ancestor
183 of BGC dividing into *mas* and *col* BGCs with a deletion event, independently.
184 Interestingly, the gene encoding major facilitator superfamily (MFS) transporter,
185 which are implicated in multidrug resistance and transport small molecules and
186 xenobiotics[23], is preserved in *col* BGC but lost in *mas* BGC. In contrast, the *masL*,
187 the acetyl-CoA acetyltransferase gene, remains in *mas* BGC but not in *col* BGC.
188 Antibiotic producers often harbor resistance genes within the antibiotic BGCs for self-
189 protection[24, 25]. On the other hand, drug resistance is also achieved by
190 amplification/overexpression of the drug target[26]. For instance, many fluconazole-
191 resistant strains of *Candida* spp. were reported to have overexpression of the drug
192 target ERG11/CYP51[6]. To evaluate the protective effect of *masL*, we first
193 constructed heterologous expression of *masL* in polyyne-sensitive *C. albicans* (P_{tet}-
194 *masL*). The expression of *masL* rescued fungal cell viability from polyyne inhibition
195 with MIC (**Fig. 3a**). Furthermore, an *in vitro* MasL inhibition assay showed that
196 polyynes (compounds **1**-**3**) inhibited the MasL enzyme activity (**Table 1**). These
197 results suggest that *masL* serves as a self-resistance gene (SRG) in the *mas* BGC,
198 and in addition that MasL could serve as a direct target of bacterial polyynes for
199 further antifungal mechanistic studies.

200

201 **Polyynes are covalent inhibitors of acetyl-CoA acetyltransferase**

202 The nucleophilic addition by covalent inhibitors targeting of the sulfhydryl group
203 of cysteine residues is the most widely utilized reaction for achieving irreversible
204 binding[27]. For instance, arecoline was reported to be an acetyl-CoA
205 acetyltransferase inhibitor using α,β-unsaturated carbonyl moieties as an electrophile
206 for the sulfhydryl group of reactive Cys126 in ACAT1 protein[28]. Moreover, (*3R*)-
207 falcarinol, which contained an internal diyne moiety isolated from the plant *Daucus*
208 *carota*, was reported to modify the chemopreventive agent-sensor Keap1 protein at
209 Cys151 covalently[29]. Therefore, we proposed a nucleophilic addition mechanism on

210 polyynes as electrophiles for the reactive cysteine sulfhydryl moiety of MasL (**Fig. 3b**)
211 and confirmed it by mass spectrometry analysis (**Supplementary Data 6**). After
212 incubating collimonin C **1**, collimonin D **2** and massilin A **3** with MasL, respectively,
213 two peptides were observed to have monoisotopic masses (within 5 ppm error)
214 consistent with Cys90 modified by Δmass +258 Da (+$C_{16}H_{18}O_3$) and 274 Da
215 (+$C_{16}H_{18}O_4$) (**Fig. 3c** and **Supplementary Fig. 6**). This observation of collimonin C/D
216 (+$C_{16}H_{18}O_4$)- and massilin A (+$C_{16}H_{18}O_3$)-derived adducts of MasL Cys90 provides
217 convincing evidence of protein S-alkylation via nucleophilic addition to the
218 conjugated terminal alkyne. Consequently, these polyyne inhibitors (compounds **1-3**)
219 represent targeted covalent inhibitors (TCIs) that selectively covalently modify an
220 essential catalytic residue in MasL, leading to irreversible inhibition.
221 The selectivity of TCI is described reasonably well by the general equation
222 (**Table 1** and **Supplementary Note**). The kinetic study showed that collimonin D **2**
223 has a lower K_I (42.84 μM) than massilin A **3** (132.10 μM) and collimonin C **1** (297.10
224 μM). This suggests that the stereochemistry of the hydroxyl group on polyynes is
225 vital for initial non-covalent complex affinity. We assume that the stereochemistry
226 also affects the reactivity of covalent complex formation for collimonin C **1** with a
227 faster k_{inact} (0.09798 min^{-1}) than collimonin D **2** (0.05208 min^{-1}) and massilin A **3**
228 (0.03449 min^{-1}). In addition, enzyme inhibition assays for acetyl-CoA
229 acetyltransferase homolog from *C. albicans* ATCC18804 ($ERG10_{L127S}$) and human
230 transition peptide-truncated ACAT1 showed that collimonin C **1**, collimonin D **2,** and
231 massilin A **3** would inhibit the enzyme activity of recombinant $ERG10_{L127S}$ and
232 ACAT1 (**Supplementary Fig. 7**). The mass spectrometry analysis of collimonin C/D-
233 and massilin A-derived adducts of $ERG10_{L127S}$ and ACAT1 also showed the polyynes
234 to be TCIs (**Supplementary Data 6**). The results showed that polyynes would modify
235 the reactive cysteine residues of acetyl-CoA acetyltransferase (Cys90/Cys382 in
236 $ERG10_{L127S}$ and Cys126/Cys413 in ACAT1). Nevertheless, polyynes would also
237 modify other cysteines with a highly nucleophilic sulfhydryl group (Cys166 in
238 $ERG10_{L127S}$ and Cys119/Cys196 in ACAT1) but not every cysteine in protein
239 (**Supplementary Fig. 8 and 9**). Taken together, polyynes as a lead structure are
240 able target the reactive cysteine residues in acetyl-CoA acetyltransferase with
241 certain selectivity.
242

243 **The MasL-collimonin C complex shares a similar interaction in the**
244 **substrate/inhibitor to enzyme binding model**

245 We solved the crystal structures of MasL in its apo and collimonin C-bound
246 forms at 1.78 Å and 1.66 Å resolution, respectively. The asymmetric unit (space
247 group *P*1 for apo MasL and $P2_1$ for complex) of both structures contains a tetramer
248 of the protein (**Supplementary Fig.10**), as observed in solution (20 mM Tris-HCl
249 pH8.5, 100 mM NaCl). The monomer of MasL shares the general fold architecture
250 reported in the type II biosynthetic thiolase family[30]. MasL consists of three domains:
251 an N-terminal α/β domain (N-domain, residues 1–121 and 251–271), a loop domain
252 (L-domain, residues 122–250), and a C-terminal α/β domain (C-domain, residues
253 272–394) (**Supplementary Fig.11)**. The N- and C-domains form a typical five-
254 layered fold (α-β-α-β-α) as observed in the structures of other type II biosynthetic
255 thiolases including *Zoogloea ramigera* PhaA[30], *Clostridium acetobutylicum*
256 CEA_G2880[31], *Aspergillus fumigatus* ERG10A[32], and human ACAT1[33]. The L-
257 domain displays an α/β fold with a tetramerization loop associated with the C-domain
258 (**Supplementary Fig.12)**.

259 Many high-resolution atomic structural models of acetyl-CoA
260 acetyltransferases/type II biosynthetic thiolases have been reported to date. The
261 structures of thiolases from many organisms are similar despite the lack of sequence
262 similarity and acyl-Co A substrate diversity. Moreover, many structural models of the
263 substrate-binding complex revealed the Claisen condensation reaction and binding
264 model within the reaction pocket. In our MasL and its complex model, the substrate-
265 binding pocket was located on the surface of the enzyme facing the opposite dimer
266 of the tetrameric assembly. The pocket was a tunnel shape of ~10 Å depth with ~6-8
267 Å diameter for the linear pantothenic moiety of coenzyme A (CoA) extending through
268 the reactive center. The Claisen condensation reactive center in MasL contained
269 reactive cysteine residues Cys90 and nucleophilic activation residues His350 and
270 Cys380 in the C-domain. In the MasL-collimonin C complex, the conjugated polyyne
271 tail extended into the MasL substrate binding site and formed a covalent bond
272 between the terminal carbon (C16) and the reactive cysteine sulfhydryl moiety of
273 Cys90 (**Fig. 4 and Supplementary Fig. 13**). The observation is consistent with
274 mass spectrometry analysis indicating the irreversible covalent inhibition of polyynes
275 on MasL or acetyl-CoA acetyltransferase/type II biosynthetic thiolases via
276 nucleophilic addition.

277 In the further analysis of the MasL-collimonin C complex, C7-OH of collimonin C
278 **1,** His158 of MasL, and a water molecule formed a strong polar interaction network,
279 including a direct hydrogen bond (3.00-3.16 Å) and a water-mediated hydrogen bond
280 between C7-OH and His158 (**Fig. 4**). The superimposition of four monomers of the
281 MasL-collimonin C complex showed that C6-OH of collimonin C **1** had more flexibility
282 on the spatial direction (with a dihedral angle to C7-OH from 109˚ to 170˚) and built a
283 sophisticated polar interaction network with the amide of Pro249 in the panthetheine
284 loop and multiple water molecules (**Supplementary Fig. 14)**. In the substrate-
285 binding model of the thiolases, the conserved histidine residue on the covering loop
286 formed a water-mediated hydrogen bond to the carbonyl moiety in the pantothenic
287 part of CoA. Also, one or more water molecules mediated the hydrogen-bonding
288 network between the hydroxyl moiety in CoA and backbone amide moieties in the
289 panthetheine loop in thiolase[34]. The polar interacting residues for the collimonin C **1**
290 (inhibitor) binding were similar to CoA (substrate) in other thiolase models therefore
291 the collimonin C **1** competitively bound into the reaction pocket.
292 The superimposition of the inhibitor/substrate binding models, including *A.*
293 *fumigatus* ERG10A (pdb code **6L2C**[32], chain A; identity 37.8%), Human ACAT1 (pdb
294 code **2IBU**[33], chain A; identity 36.8%), *C. acetobutylicum* CEA_G2880 (pdb code
295 **4XL4**[31], chain A; identity 48.9%) and *Z. ramigera* PhaA (pdb code **1QFL**[30], chain A;
296 identity 44.6%), showed that collimonin C **1** could align well with the phosphate-
297 pantothenic part of CoA (**Fig. 5**). The hydrogen bond between C7-OH of collimonin C
298 **1** and His158 of MasL was well superimposed with the polar interaction of carbonyl
299 moiety in CoA. Even though the superimposition between C6-OH of collimonin C **1**
300 and the α-hydroxy pantoic acid moiety showed a slightly different polar network
301 orientation due to hydroxyl moiety flexibility, the polar interaction was still conserved
302 in the substrate/inhibitor binding model. The crystallographic analysis and *in vitro*
303 thiolase activity assay demonstrated that the configuration of hydroxyl moiety of
304 polyynes is vital for enzymatic affinity.
305 Surprisingly, although there was no significant induced-fit within the pocket, the
306 collimonin C **1** caused the Arg135 on the tetramerization loop to swap to form a salt
307 bridge across the two subunits within the binding site (**Supplementary Fig. 15)**. This
308 finding was similar to the CoA-bound thiolase in *C. acetobutylicum* CEA_G2880 (pdb
309 code **4XL4** [31]), in which the Arg133 in CEA_G2880 formed a hydrogen bond to the
310 phosphate moiety of CoA. The salt bridge/hydrogen bond formation on the arginine

311 in thiolase would increase the binding affinity and suggests that collimonin C **1** would
312 stabilize the tetramer of MasL rather than disrupting the tetramerization of ACAT1 as
313 arecoline inhibition[28].
314
315 **Acetyl-CoA acetyltransferase as an antifungal target**
316 In this study, we confirmed that collimonin C **1**, collimonin D **2,** and massilin A **3**
317 would inhibit the enzyme activity of acetyl-CoA acetyltransferase homolog
318 $ERG10_{L127S}$ from *C. albicans* through covalent competition on the substrate binding
319 site and the reactive cysteine residue. As acetyl-CoA acetyltransferase is the first
320 enzyme to catalyze acetoacetyl-CoA formation for mevalonate biosynthesis,
321 inhibition of $ERG10_{L127S}$ would block the mevalonate production and subsequently
322 disrupt the squalene and ergosterol biosynthesis. Among the clinical antifungal drugs,
323 azole drugs inhibit ergosterol biosynthesis by targeting the critical biosynthesis
324 enzyme ERG11 and causing the dysfunction of maintenance of fluidity, permeability,
325 and structural integrity of fungal cell membrane[4]. Moreover, the reduced expression
326 of acetyl-CoA acetyltransferase homolog ERG10A in *A. fumigatus* led to severe
327 morphological defects and increased susceptibility to oxidative and cell wall
328 stresses[32]. Therefore, we carried out a transmission electron microscopy experiment
329 and observed that polyynes disrupt the cell membrane structure (**Fig. 6a**).
330 Meanwhile, we detected that *ERG10* gene expression was upregulated during
331 co-culture of *Massilia* sp. YMA4 with *C. albicans* (**Fig. 6b**). Furthermore, we
332 constructed the *ERG10* overexpression strain of *C. albicans* (P_{tet}-*ERG10*). We found
333 that the overexpression of *ERG10* could rescue the fungal cell viability from polyyne
334 inhibition with MIC as a protective effect of heterologous expression of *Massilia* sp.
335 YMA4 *masL* in *C. albicans* (**Fig. 6c**). Taken together, these results revealed the
336 antifungal mechanism of the polyynes (compounds **1-3**) through targeting the acetyl-
337 CoA acetyltransferase ERG10, resulting in *C. albicans* inducing expression of
338 *ERG10* for tolerance to *Massilia* sp. YMA4 attack during fungal-bacterial interaction.
339
340 **Discussion**
341 After the Waksman platform was first introduced in the 1940s[35], many natural
342 antibiotics were systematically discovered in the chemical crosstalk of microbe-
343 microbe interaction. Even though recent technology can rapidly explore the
344 metabolites hidden in the interaction between host and effector, environmental

345 factors have a significant impact on antibiotic production resulting in various
346 bioactive spectra, which should be considered in practical surveys. *Massilia* sp.
347 YMA4 showed differential antifungal activity in response to different culture
348 conditions. However, the antifungal activity of *Massilia* sp. YMA4 extract was too
349 unstable to identify the active metabolites using the general bioactivity-guide
350 isolation approach. Because of this, we instead combined transcriptomics, functional
351 genetics, and metabolomics analyses to reveal the *mas* BGC and its products—
352 unstable bacterial polyynes—as the principal antifungal agents of *Massilia* sp. YMA4.
353 We succeeded in identifying two new compounds, massilin A **3** and B **4**, and two
354 known compounds, collimonins C **1** and D **2**. Massilin B **4,** the potential precursor of
355 collimonin C **1** or D **2,** did not contain the terminal alkyne and was more stable than
356 other terminal alkyne-containing polyynes but lost its antifungal activity. This
357 chemical property had been mentioned in the study of *Pseudomonas protegens*,
358 which protegenins C **12** and D **13** without terminal alkyne are more stable than
359 protegenins A **10** and B **11** but the antioomycete activities against *P. ultimum* are
360 greatly reduced [21].

361 Notably, the critical terminal alkyne of bacterial polyynes had been mentioned in
362 the study of *Pseudomonas protegens*. This implies that the terminal alkyne of
363 bacterial polyynes is a prerequisite for bioactivity and a contributor to their instability,
364 resulting in self-polymerization.

365 Previous reports of polyyne BGCs discovered through transposon mutagenesis
366 gave partial information for characterizing the complete BGC architecture[9, 11]. During
367 the genome mining of *mas* BGC, we failed to use the rule-based genome mining
368 tools (antiSMASH[16]) to recognize the cluster information due to the lack of defined
369 polyyne BGC information. However, the deep learning genome mining tool
370 (DeepBGC [17]) classified *mas* BGC as a type II fatty acid/polyketide synthase (FA-
371 PKS) BGC [36] with indicative features, such as fatty acyl-AMP ligase (FAAL), an acyl
372 carrier protein (ACP), fatty acid desaturases (FADs) and hydrolases/thioesterase
373 (H/TE). Subsequently, combining the genome mining and transcriptomics analysis
374 results, the putative BGC was correlated to complete the characterized *mas* BGC.
375 Further information about the polyyne BGCs was attained out by blasting multiple
376 homologs using MultiGeneBlast[18] with a fully transcribed *mas* BGC as a query. The
377 BGC mining results helped us figure out the core biosynthesis architecture in
378 polyyne BGC as an arranged feature of FAAL-2x FAD-ACP-FAD-H/TE. The

379 subsequent phylogenetic analysis for the polyyne BGCs by conserved core genes
380 combined with chemotaxonomy revealed that a potential evolutionary event,
381 substrate-specific functional evolution (palmitate and stearate) occurred prior to
382 spreading inter-species.

383 Antibiotics encoding BGCs are important as a defensive strategy for microbial
384 survival. Plasmids are common carriers for BGC transformation between bacteria to
385 gain functional genes. In addition, horizontal gene transfer (HGT) [37] is another
386 strategy of gene transfer and usually occurs in bacteria to gain function to defeat
387 enemies. Regarding the relationship within a sister group of polyyne BGCs in
388 palmitic-derived monophylum (*ccn* encoding cepacins and *col* encoding collimonins),
389 HGT events hypothetically transmitted polyyne BGC from *ccn* BGC into *mas* and *col*
390 BGCs, independently. Then, a deletion event occurred with the result that the *ccn*
391 BGC independently divided into *mas* BGC and *col* BGC each of which contained a
392 different self-protection mechanism. The *col* BGC preserved the MFS transporter
393 and, in contrast, *mas* BGC kept the acetyl-CoA acetyltransferase (MasL) for
394 detoxification in polyyne production.

395 In drug-target surveys, the inhibitor target has sometimes been found to serve a
396 protective function to resist the inhibitor[38, 39]. In this study, we identified the acetyl-
397 CoA acetyltransferase MasL as the direct target of the polyynes, and the homolog
398 ERG10 in *C. albicans* could gain resistance by overexpression. This suggests that
399 ERG10 is the antifungal target of polyynes disrupting the mevalonate and
400 downstream ergosterol biosynthesis, and then abolishing the cell membrane integrity.
401 The success in this case reintroduces the notion that drug targets can be discovered
402 from screening the SRG in gain-of-function assay. Moreover, inhibition of human
403 mitochondrial acetyl-CoA acetyltransferase ACAT1 by the bioactive polyynes
404 (compounds **1-3**) suggested that polyynes would be a species-wide inhibitor of
405 acetyl-CoA acetyltransferases/type II biosynthetic thiolases.

406 The mevalonate pathway metabolites are essential for cancer cell survival and
407 growth, for example, ketogenesis is associated with prostate cancer progression[40].
408 Likewise, statins, the hypercholesterolemia drugs also showed anticancer effects on
409 stem cell-like primary glioblastoma by inhibiting HMG-CoA reductase in mevalonate
410 biosynthesis[41]. ACAT1, the first enzyme of the mevalonate biosynthesis pathway,
411 was reported to be an important factor for tumor growth in multiple cancer cell lines[28].

412 As we revealed that bacterial polyynes could inhibit human mitochondrial ACAT1, it
413 would be worth exploring the anticancer potential of bacterial polyynes in the future.
414 To date, acetyl-CoA acetyltransferase inhibitors have usually been designed as
415 CoA substrate derivatives or analogs (**Supplementary Fig.16**). Notably, the binding
416 affinity (Km) of acetyl-CoA acetyltransferase with CoA-derivate substrates ranges
417 from 3.8 μM to 1.06 mM [32]. Compared to previous analog inhibitor reports, in which
418 K_I ranged from 1.4 μM to 15 mM and k_{inact} ranged from 0.26 min^{-1} to 4 min^{-1},
419 bioactive polyynes in our study inhibited MasL with an equal level of binding affinity
420 (K_I from 42.84 μM to 297.10 μM) but lower reaction rate (k_{inact} from 0.03 min^{-1} to 0.1
421 min^{-1})[42, 43, 44]. These data suggest polyynes may be a potential lead structure for drug
422 design.
423 In covalent drug design, inhibitors with an electrophile moiety, such as nitrile,
424 alkyne, acrylamide, epoxide, or α,β-unsaturated carbonyl, are the major resources
425 for covalent bond formation to the nucleophilic moieties[27]. For example, falcarindiol
426 was reported to have S-alkylation at Cys151 in Keap1 protein[29]; however, it lacks an
427 actual bond formation mechanism. Polyynes are a group of high electron enriched
428 metabolites that usually react to nucleophilic moieties. In the MasL-collimonin C
429 complex model, the terminal alkyne of polyynes was used to elaborate bond
430 formation with the sulfhydryl moiety in MasL Cys90. Furthermore, we revealed
431 structurally detailed substrate/inhibitor binding models of the thiolases. The
432 superimposition of the MasL-collimonin C complex and the other CoA-thiolase
433 complexes showed collimonin C **1** and CoA shared a similar polar interaction to bind
434 to the thiolases. Additionally, regarding the salt bridge/hydrogen bond formation
435 within the binding site, the induced-fit arginine/lysine residue was conserved in
436 procaryotic species but not in eukaryotic homologous thiolases. This supposedly
437 causes a different affinity in homologous thiolases and could highlight ligand-based
438 drug design with species selectivity.
439 In summary, we used an integrated strategy to unveil the biosynthesis and
440 antifungal mechanism of bacterial polyynes. A well-characterized core architecture of
441 bacterial polyyne BGC was attained which allowed the exploration of new bacterial
442 polyynes further using genome mining. We illustrated the antifungal mechanism of
443 collimonin C **1**, collimonin D **2**, and massilin A **3** through inhibiting the acetyl-CoA
444 acetyltransferase ERG10 in *C. albicans*. The crystallographic analysis provided
445 detailed structural insight into the MasL-collimonin C complex, which will provide

446 useful information for designing new inhibitors of acetyl-CoA acetyltransferase.
447 These results will help future research in bacterial polyyne mining, biosynthesis, and
448 the structure-activity relationship to develop new antifungal or anticancer drugs.
449
450 **Methods**
451 **Genome mining and phylogenetic analysis of polyyne biosynthesis gene**
452 **clusters**
453 The biosynthesis gene clusters (BGCs) in the genome of *Massilia* sp. YMA4
454 were characterized via command-line program DeepBGC[17] and online software
455 antiSMASH[16] with default settings, and integrated with the criteria: antiSMASH score
456 > 1500, DeepBGC score > 0.7. Then, the *mas* BGC of *Massilia* sp. YMA4 was used
457 to discover the homologous gene clusters in bacteria species using MultiGeneBlast[18].
458 The database was built with a bacterial sequences database (BCT, 2020 December
459 01) and whole-genome sequences of polyyne-reported bacterial species from NCBI.
460 A total of 56 bacteria with polyyne BGC (Cumulative Blast bit score > 1500) were
461 found. The homologous protein sequences of each bacterial polyyne BGC were
462 respectively concatenated (total of five amino sequences, starting from MasD
463 homolog to MasI homolog). The concatenated protein sequences were used for
464 alignment (MUSCLE) and the distance (UPGMA, bootstrap 5000 times) between 56
465 bacteria with *Massilia* sp. YMA4 was identified for phylogenetic tree construction.
466 The analysis was completed by using MEGA 10 with default parameters[45]. iTOL was
467 used to present the results of phylogenetic analysis[46].
468
469 **Mass spectrometry analysis and peptide mapping of polyyne-labeled peptides**
470 **in MasL, ERG10$_{L127S}$, and ACAT1**
471 Incubation mixture (20 μL) containing 2 μM protein in 50 mM Tris pH 8.5, 100
472 mM NaCl, was incubated with 40 μM collimonin C **1**, collimonin D **2**, or massilin A **3**
473 at 25°C for 3 h. The reaction was quenched by adding 4x Laemmli sample buffer
474 (Bio-Rad, USA) with 5 mM DL-dithiothreitol and the protein was separated using
475 SDS-PAGE. The in-gel trypsin digestion was performed with a substrate-to-enzyme
476 ratio of 25:1 (w/w), and the mixture was incubated at 37°C for 20 h[47]. The resultant
477 peptide mixtures were dried and frozen at -20°C until separation by reverse-phase
478 nanoUPLC-ESI-MS. The tryptic peptides were re-dissolved in 10 μL of 0.1% formic

479 acid. An LC-nESI-Q Exactive mass spectrometer (Thermo Scientific, USA) coupled
480 with an online nanoUPLC (Dionex UltiMate 3000 Binary RSLCnano) was used for
481 analysis. An Acclaim PepMap 100 C18 trap column (75 μm x 2.0 cm, 3 μm, 100 Å,
482 Thermo Scientific, USA) and an Acclaim PepMap RSLC C18 nanoLC column (75 μm
483 x 25 cm, 2 μm, 100 Å) were used with a linear gradient from 5% to 35% of
484 acetonitrile in 0.1% (v/v) formic acid for 40 min at a flow rate of 300 nL/min. The MS
485 data were collected in the data-dependent mode with a full MS scan followed by 10
486 MS/MS scans of the top 10 precursor ions from the full MS scan. The MS scan was
487 performed with 70,000 resolution over the mass-to-charge (*m/z*) range 350 to 1600,
488 and dynamic exclusion was enabled. The data-dependent MS/MS acquisition was
489 performed with a two *m/z* isolation window, 27% normalized collision energy, and
490 17,500 resolution.
491 The data were processed using Proteome Discoverer (version 2.4; Thermo
492 Scientific, USA), and the peptides were identified by searching the MS/MS spectra
493 against the MasL, $ERG10_{L127S,}$ and ACAT1 using the Mascot search engine (version
494 2.3; Matrix Science, UK) and SEQUEST search engine[48]. Cysteine alkylation was
495 used as a dynamic modification, and the modification *m/z* values were +274.121
496 (+$C_{16}H_{18}O_4$ for collimonin C/D) and +258.126 (+$C_{16}H_{18}O_3$ for massilin A),
497 respectively. For identification, the false discovery rate was set to 0.01 for peptides,
498 proteins, and sites. The minimum peptide length allowed was four amino acids,
499 precursor mass tolerance for 10 ppm, and fragment mass tolerance for 0.02 Da.
500
501 **Enzymatic inhibition assay and inhibition kinetics of polyynes**
502 The enzymatic inhibition assay was initiated by adding 50 μM polyynes
503 (collimonin C **1**, collimonin D **2,** and massilin A **3**) into 10 μM $ERG10_{L127S}$ or ACAT1
504 at 25°C for 1 h. The residue active enzyme reaction started by adding 10 mM acetyl-
505 CoA for another 1 h at 25°C in a total of 12 μL volume with the following
506 concentrations: 8.33 μM enzymes, 41.65 μM polyynes, and 1.67 mM acetyl-CoA.
507 The reaction was quenched by adding 1 μL of 1% formic acid. The monitor method
508 of releasing CoA using a fluorescent probe (7-diethylamino-3-(4-maleimidophenyl)-4-
509 methylcoumarin, CPM) was modified from previous research[49]. The released CoA
510 was used to represent the residual activity or protein occupancy. After 10 min, the
511 pH value was adjusted by 2 μL 0.1 M Tris pH10 and 100 μM CPM probe was added
512 in a total volume of 105 μL for 30 min reaction at 30°C followed by detection of the

513 fluorescent signal using a BioTek Synergy H1 microplate reader (excitation 355 nm;
514 emission 460 nm). Relative fluorescence intensity was obtained by subtracting the
515 fluorescence intensity of the polyyne-free reaction system.
516 To measure the inhibition kinetics of the polyynes to MasL, different polyyne
517 concentrations as indicated were reacted with the protein for inhibition reaction and
518 then enzymatic reaction as described above. Protein occupancy and inhibition kinetic
519 calculations were performed using GraphPad Prism8 (GraphPad Software, USA; see
520 details in the **Supplementary Notes**).
521
522 **Protein Crystallization, Data Collection, Processing, and Refinement**
523 For MasL-collimonin C complex preparation, 20 μM MasL was incubated with
524 100 μM collimonin C in 20 mM Tris-HCl pH 8.5, and 100 mM NaCl. The MasL-
525 collimonin C complex was purified with a gel-filtration (Superdex 200 Increase
526 10/300) column.
527 A freshly thawed aliquot of MasL and MasL-collimonin C complex was
528 concentrated to 20 mg/ml for an initial crystallization screening of ca. 500 conditions
529 (Academia Sinica Protein Clinic, Academia Sinica). The crystallization conditions
530 were manually refined to the final conditions: for MasL, 2% (v/v) Tacsimate pH 7.0,
531 16% (w/v) polyethylene glycol 3,350, and 0.1 M HEPES, pH 7.5; for MasL-collimonin
532 C complex, 20% (w/v) polyethylene glycol 3,350 and 0.2 M tri-lithium citrate, pH 8.
533 The crystals were grown at 10°C by mixing the protein aliquot with an equivalent
534 volume of crystallization buffer via the hanging drop vapor-diffusion method. For X-
535 ray data collection, the crystals were immediately flash-frozen in liquid nitrogen after
536 dipping into cryoprotectant composed of crystallization solution supplemented with
537 10% (v/v) glycerol.
538 X-ray diffraction experiments were conducted at 100K at the TLS beamline 15A
539 or the TPS beamline 05A of the National Synchrotron Radiation Research Center
540 (Hsinchu, Taiwan) with a wavelength of 1 Å. All diffraction data were processed and
541 scaled with the HKL-2000 package[50]. The data collection statistics are listed in **Table**
542 **2**. The resulting MasL crystals had a space group of *P*1 with four MasL molecules in
543 an asymmetric unit and a solvent content of ca. 56%. The MasL-collimonin C
544 complex crystals had a space group of $P2_1$ with one asymmetric unit containing four
545 MasL molecules and a solvent content of ca. 51%[51].

546 The structures of MasL and MasL-collimonin C complex were solved by the
547 molecular replacement method with the program Molrep[52] using the structure of
548 thiolase from *Clostridium acetobutylicum* (pdb code **4N44**) as the search model.
549 Computational model building was conducted with ARP/wARP or Buccaneer[53, 54,
550 and the rest of the models were manually built with Coot.[55] The resulting models
551 were subjected to computational refinement with Refmac5.[56]
552 The collimonin C and well-ordered water molecules were located with Coot. The
553 stereochemical quality of the refined models was checked with MolProbity[57]. Finally,
554 the MasL and MasL-collimonin C complex's refinement converged at a
555 final R factor/R_{free} of 0.128/0.180 and 0.114/0.162, respectively. The final refinement
556 statistics are listed in **Table 2**. The refined models of MasL and MasL-collimonin C
557 complex were deposited in the Protein Data Bank with pdb_codes **7EI3** and **7EI4**,
558 respectively. The molecular figures were produced with Maestro (**Schrödinger
559 Release 2021-1**: Maestro, Schrödinger, LLC, USA).
560
561 **Minimum inhibitory concentration determination and genetic rescue assay**
562 The minimum inhibitory concentration (MIC) measurement was modified from R
563 J Lambert's method[58]. Different concentrations (300.00, 150.00, 75.00, 37.50, 18.75,
564 9.38, 4.69, 2.34, 1.17, 0.59, 0.29 μM) of collimonin C **1**, collimonin D **2**, massilin A **3**,
565 atorvastatin, and amphotericin B were prepared in yeast extract-peptone-dextrose
566 (YPD). The *C. albicans* cell viabilities were seeded with initial O.D. 0.05 (600 nm)
567 and incubated at 37˚C. After 24 h incubation, the final O.D. was recorded by Epoch 2
568 Microplate (BioTek Instruments, USA) for MIC calculation.
569 For genetic rescue assay, the *ERG10* overexpression and *masL* heterologous
570 expression strains were seeded with O.D. 0.05 at 600 nm in YPD treated with MIC of
571 each polyyne at 37˚C and supplied with 40 μg/mL doxycycline for gene expression.
572 The *C. albicans* cell viabilities were recorded at 24 h.
573 The experimental results include at least three biological replicates, and the cell
574 viabilities were normalized to the mock treatment. The statistical results were
575 analyzed using GraphPad Prism 8 (GraphPad Software, USA) with multiple t-test
576 analyses (FDR < 0.05). The MIC of polyynes was built with cell viability (%) of
577 different concentrations, fitting into the modified Gompertz function[58].
578

Data availability

The genome was deposited into the NCBI BioProject database under accession PRJNA476678. The raw-reads of RNA sequencing were deposited at the Sequencing Read Archive (BioProject: PRJNA706894). All LC-MS data used in this paper are publicly available at the GNPS-MassIVE repository under the accession MSV000087007. The raw data of bottom analysis are publicly available at the GNPS-MassIVE repository under the MassIVE accession MSV000087027. The coordinates and structural factors have been deposited with the Protein Data Bank under accession codes **7EI3** (MasL) and **7EI4** (MasL-Collimonin C complex)

Acknowledgments

We thank Dr. Chao-Jen Shih (Bioresource Collection and Research Center, Taiwan) for isolating and identifying *Massilia* sp. YMA4. The materials and methods for the construction of biosynthetic gene-null mutant strain were generously provided by Prof. Nai-Chun Lin's Lab (National Taiwan University, Taiwan). We thank Prof. Ching-Hsuan Lin and Ms. Chih-Chieh Hsu (National Taiwan University, Taiwan) for providing clinical *Candida* strains and the material for the construction of tetracycline-inducible expression system. We thank Dr. Pei-Wen Hsiao (Agricultural Biotechnology Research Center, Academia Sinica, Taiwan) for providing human prostate PC-3 cell line for cloning ACAT1 gene. We thank Mr. Ning Lu, Ms. Ying-Mi Lai, and Ms. Chia-Chi Peng for collecting preliminary data. NMR data were collected in the High Field Nuclear Magnetic Resonance Center, Academia Sinica. LC-MS data were collected in the Metabolomics Core Facility, Agricultural Biotechnology Research Center, Academia Sinica, and the Proteomics Core Laboratory, Institute of Plant and Microbial Biology, Academia Sinica. TEM data were collected in the Biological Electron Microscopy Core Facility, Academia Sinica. The EM core facility is funded by the Academia Sinica Core Facility and Innovative Instrument Project (AS-CFII-108-119). We further thank the Protein Crystallization Facility (Academia Sinica Protein Clinic, Academia Sinica) for assistance in crystallization preparation; and the National Synchrotron Radiation Research Center (Hsinchu, Taiwan) with beamlines TLS 15A and TPS 05A in the for assistance in X-ray data collection and access to the synchrotron radiation centers.

Author contributions

C.-C.L., S.Y.H., C.L., C.-H.S., H.-J.L., P.-Y.C., L.-J.S., B.-W.W., and W.-C.H. performed the experiments. C.-C.L., S.Y.H., K.-F.H., and Y.-N.H. carried out the data analysis. C.-C.L and S.Y.H. wrote the manuscript. Y.-L.Y. supervised the study. Y.-L.Y acquired funding to support the work.

Funding

This research was funded by the Ministry of Science and Technology of Taiwan (MOST 104-2320-B-001-019-MY2)

Competing interests

The authors declare no competing interests.

Additional information

Supplementary information The online version contains supplementary material available at xxxxxxx

The supplementary data descriptions as following:

Supplementary Data 1: RNA-seq analysis for different culture media by CLC workbench.

Supplementary Data 2: KEGG pathway analysis of DEG from RNA-seq analysis.

Supplementary Data 3: *In silico* prediction of biosynthetic gene clusters in *Massilia* sp. YMA4 by DeepBGC and antiSMASH.

Supplementary Data 4: MultiGeneBlast results of *mas* BGC query in BCT database.

Supplementary Data 5: Phylogenetic tree of bacterial polyyne biosynthetic gene clusters.

Supplementary Data 6: Bottom-up proteomics data of polyyne-modification proteins.

642 **Figures and Tables**

643

644 **Table 1 | Antifungal activity of polyynes and their inhibition kinetics to MasL of**
645 ***Massilia* sp. YMA4**

Polyynes	MIC (μM)[a]	K_I (μM)[b]	k_{inact} (min^{-1})[b]	k_{inact} / K_I ($\mu M^{-1} min^{-1}$)[b]
Collimonin C **1**	69.73	297.10	0.09798	0.000330
Collimonin D **2**	35.24	42.84	0.05208	0.001216
Massilin A **3**	2.40	132.10	0.03449	0.000261
Massilin B **4**	>500	-	-	-

646 [a]Minimum inhibitory concentration (MIC) for *C. albicans* (**Supplementary Fig. 5**).
647 [b]Experimental details and statistics are provided in the **Supplementary Notes.**

648 **Table 2 | Data collection and refinement statistics**

	MasL	MasL-collimonin C complex
Data collection		
Space group	*P*1	$P2_1$
Cell dimensions		
a, *b*, *c* (Å)	71.786, 76.995, 98.082	59.139, 115.077, 125.789
α, β, γ (°)	79.77, 79.00, 62.98	90.00, 91.08, 90.00
Resolution (Å)	30.0-1.78 (1.84-1.78)	30.0-1.66 (1.72-1.66)
R_{merge}	0.045 (0.233)	0.082 (0.560)
$I / \sigma I$	23.8 (5.0)	17.7 (2.0)
Completeness (%)	92.3 (85.2)	99.4 (94.4)
Redundancy	3.8 (3.9)	5.6 (4.8)
Refinement		
Resolution (Å)	29.9-1.78	29.2-1.66
No. reflections	160,857	180,941
R_{work} / R_{free}	0.128/0.180	0.114/0.162
No. atoms		
Protein	11,522	11,544
Ligand/ion	-	80
Water	1,663	1,720
B-factors		
Protein	22.3	18.3
Ligand/ion	-	44.0
Water	34.9	34.1
R.m.s. deviations		
Bond lengths (Å)	0.008	0.009
Bond angles (°)	1.455	1.449

649 * Highest-resolution shell is shown in parentheses

650

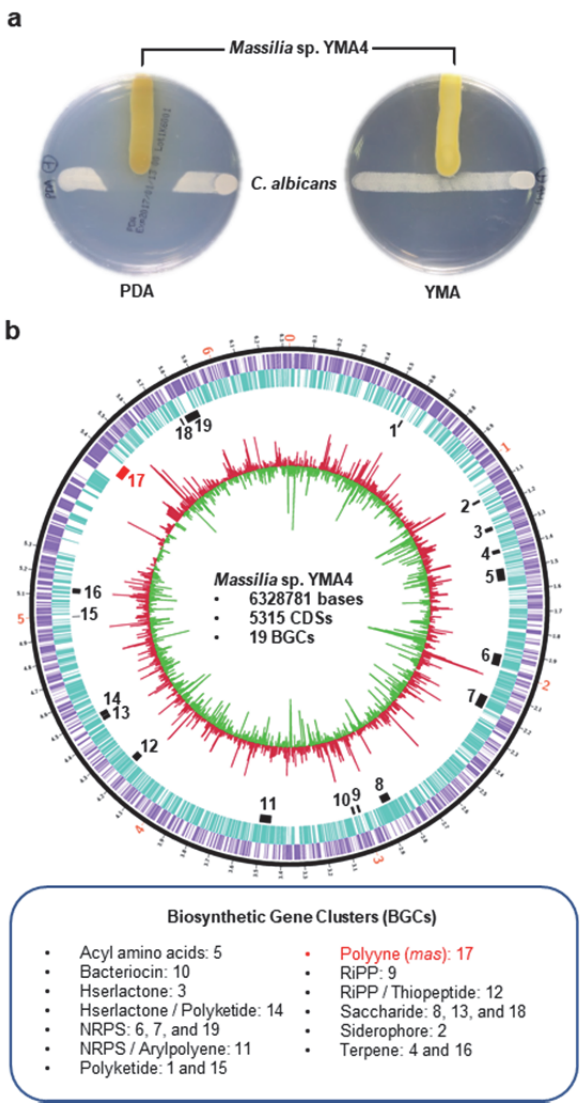

Fig. 1 Differentiation of antifungal phenotype and differential expression of biosynthetic gene clusters of *Massilia* sp. YMA4. (**a**) Antagonism assay of *Massilia* sp. YMA4 against *C. albicans* on PDA (active) and YMA (inactive) media. (**b**) Whole-genome sequence and RNA-seq analysis of *Massilia* sp. YMA4 on PDA (active) and YMA (inactive) media. Megabases are labeled as red on the outer black track; smaller ticks correspond to 100 kbp segments. The circular tracks from outside to inside represent: (1) coding sequences (CDSs) on the forward strand (purple); (2) CDSs on reverse strand (blue); (3) predicted biosynthetic gene clusters (BGCs, black and red) and polyyne BGC (red); (4) fold change histogram of CDSs of *Massilia* sp. YMA4 on PDA versus YMA; red indicates upregulation, and green indicates downregulation.

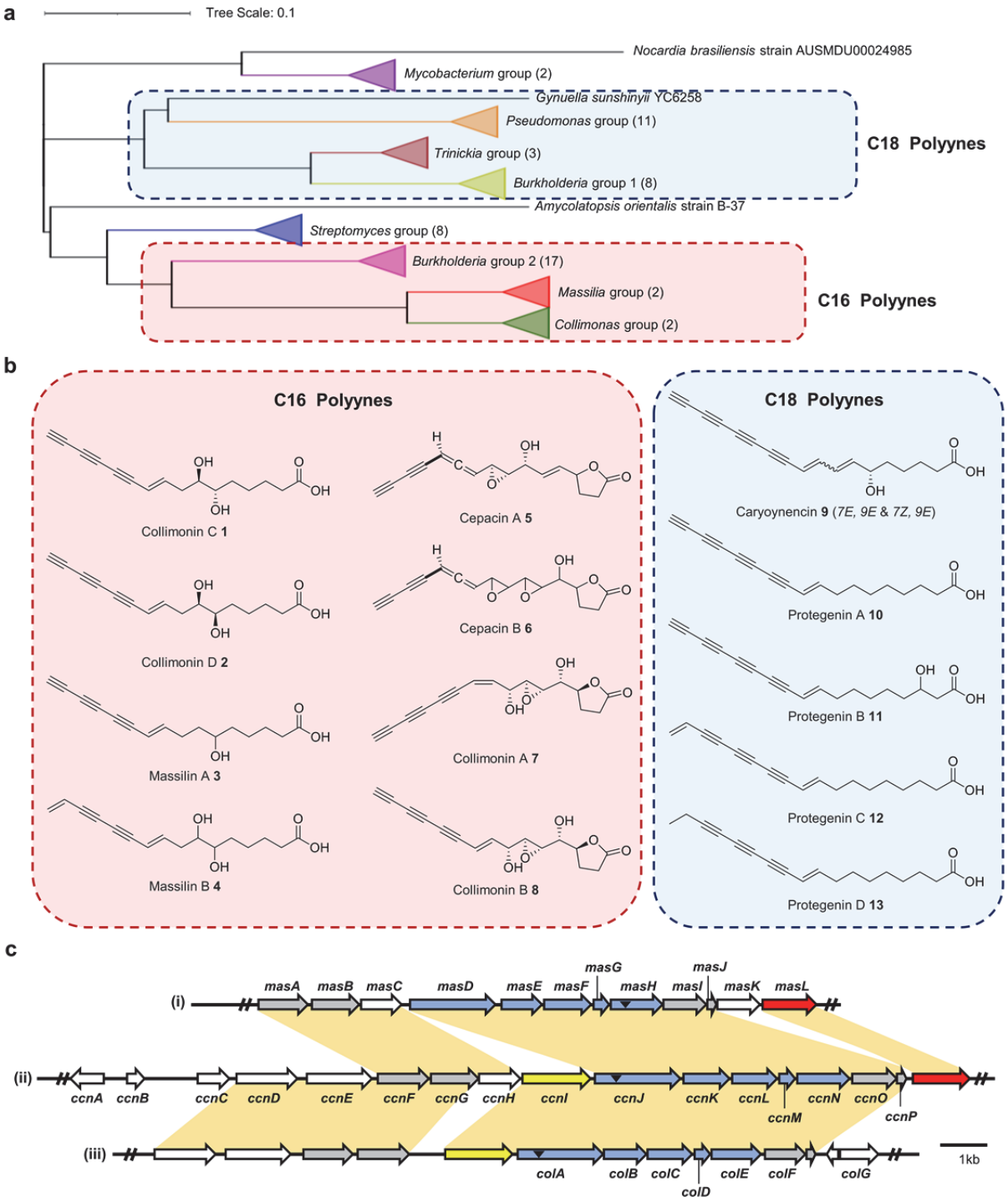

Fig. 2 Comparative analysis of polyyne biosynthetic gene cluster (BGC) and structures of bacterial polyynes. (**a**) Phylogenetic analysis of polyyne BGCs in 56 bacteria genomes. The polyyne BGCs were mined in the NCBI BCT database (2020 version) through protein sequence homology using polyyne BGC of *Massilia* sp. YMA4 (*masA* to *masL*) as a query by MultiGeneBlast[18]. Species in the blue boxes have been reported to produce C18 polyynes and species in the red boxes have been reported to produce C16 polyynes. The phylogenetic tree was built with

concatenated protein sequences of the gene cluster's conserved region (*masD* to *masI*) using MUSCLE alignment algorithm and distance estimated with 5000 bootstraps of UPGMA method in MEGA 10[45]. (**b**) The chemical structures of C16 and C18 polyynes [9, 10, 11, 19, 21], Collimonin C **1**, collimonin D **2,** and new compounds massilin A **3,** massilin B **4** were found in *Massilia* sp. YMA4. (**c**) Comparison of the polyyne BGC architectures of *Massilia* sp. YMA4 massilins (**i**), *B. ambifaria* BCC0191 cepacins [9] (**ii**), and *C. fungivorans* Ter331 collimonins [11] (**iii**). Genes conserved in polyyne BGCs across the phylogenetic tree are colored blue and those conserved in C16 polyyne monophylum are colored gray. The potential protective genes in BGC are colored red for acetyl-CoA acetyltransferase and yellow for MFS transporter. The corresponding homolog (over 40% identity) in BGCs between the two species are shown in the green area. Black triangles indicate the mutation sites in previous research and this study.

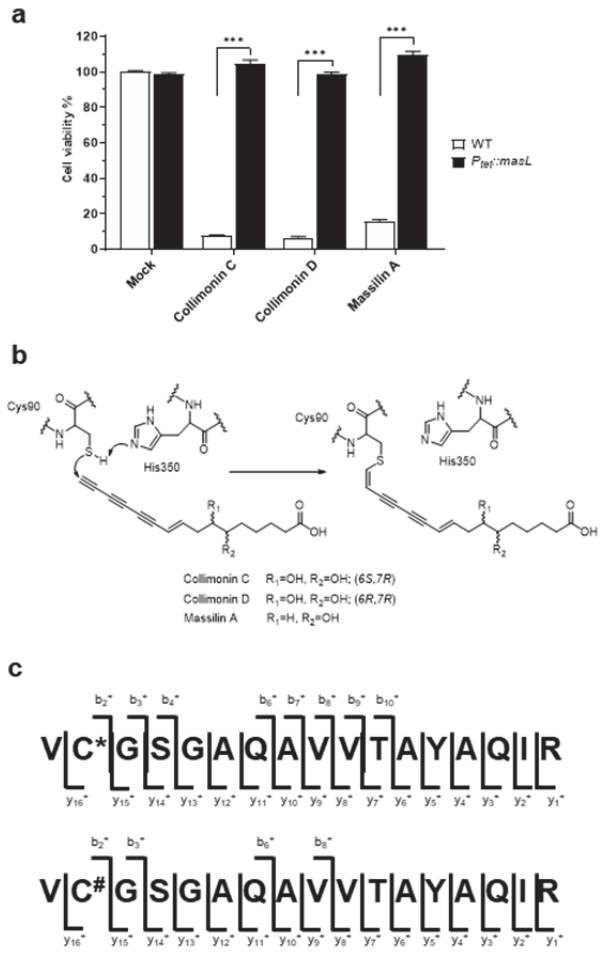

Fig. 3 Polyynes as electrophiles for thiol−alkyne addition target MasL active cysteine residue for irreversible covalent inhibition. (**a**) *C. albicans* were rescued by overexpression of *Massilia* sp. YMA4 *masL* from the minimum inhibitory concentration of polyyne treatment. The standard deviation was calculated based on three replicates and the Student t-test was used for statistical analysis. ***, $P < 0.001$. (**b**) The proposed nucleophilic addition mechanism of polyynes (with terminal alkyne) and MasL via S-alkylation of Cys90. (**c**) Mass spectrometry analysis of the polyynes-derived covalent modification on MasL Cys90 (as indicated by Δ mass +258 (asterisks) Da for massilin A **3** and +274 (hash mark) Da for collimonin C/D **1**, **2**). (see details in **Supplementary Fig. 8**).

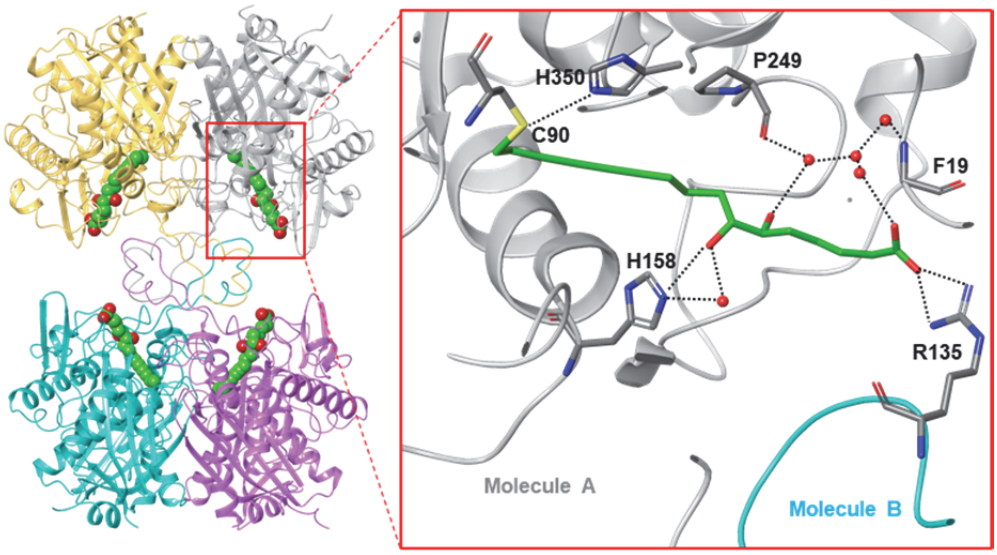

Fig. 4 Modeled structures of MasL-collimonin C complex and polar interaction within the binding site. Representative views of the crystal structures of MasL in complex of collimonin C **1**. The residues involved in collimonin C **1** interactions are shown as sticks with sequence identities indicated in the main chain molecule in gray and Arg135 in another molecule in cyan color. The dotted lines indicate the hydrogen bonds and salt bridge involved in collimonin C **1** interactions within the binding pocket.

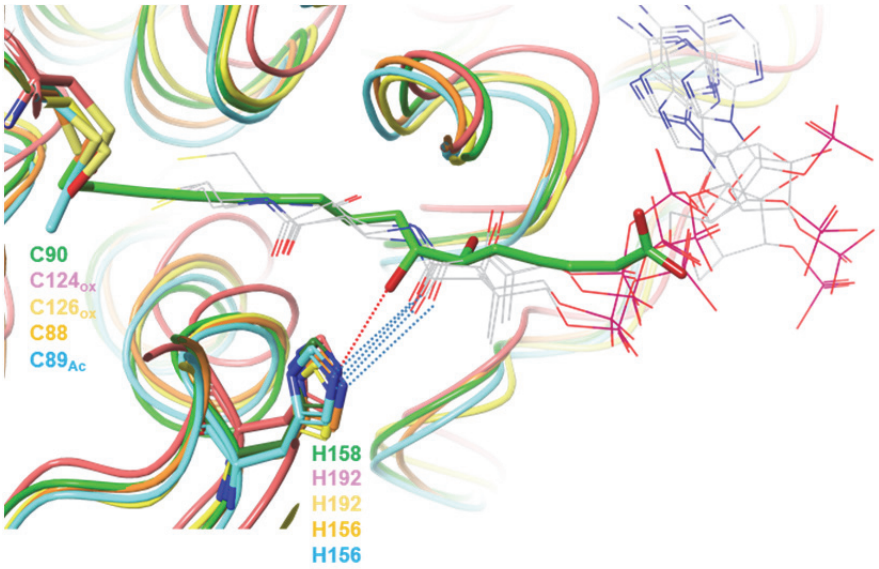

706

707 **Fig. 5 Structure comparison with ligand-bound acetyl-CoA acetyltransferase.**
708 Superposition of enzyme monomers of *Massilia* sp. YMA4 MasL bound to Collimonin
709 C **8** (pdb code **7EI4**, chain A; green) and *A. fumigatus* ERG10A (pdb code **6L2C**,
710 chain A[32]; salmon), Human ACAT1 (pdb code **2IBU**, chain A[33]; yellow), *C.*
711 *acetobutylicum* CEA_G2880 (pdb code **4XL4**, chain A[31]; orange), *Z. ramigera* PhaA
712 (pdb code **1QFL**, chain A[30]; cyan) bound to CoA. The conserved histidine residues
713 involved in polar interactions are shown as sticks, with sequence identities colored
714 the same as the backbone shown as a ribbon. All CoA ligands are shown with
715 carbon atoms in gray as lines; while collimonin C **1** is shown with carbon atoms
716 green as sticks. The red dotted line indicates the hydrogen bonds in the MasL-
717 collimonin C complex. The blue dotted lines indicate the water-mediated polar
718 interactions between CoA and selected histidine residues. Abbreviations for active
719 cysteine modification: Ox, oxidized form of the cysteine thiol group (sulfenic acid
720 type); Ac, acetylation of the cysteine residue.

721

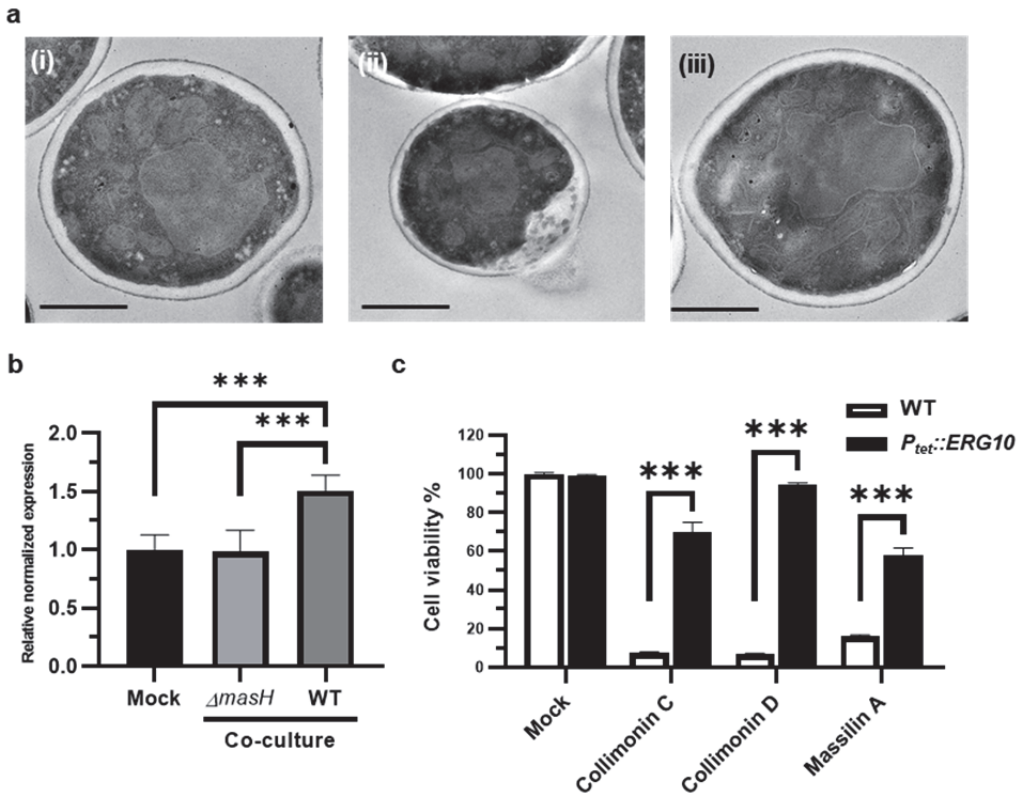

722

723 **Fig. 6 Polyynes inhibit *C. albicans* through disruption of cell membrane**
724 **stability.** (**a**) Transmission electron microscopy images of *C. albicans* cells treated
725 with Mock (**i**) and 1 mg/mL *Massilia* sp. YMA4 ethyl acetate crude extract (**ii**). Cells
726 treated with 1 mg/mL Δ*masH* ethyl acetate crude extract (**iii**) were used as a
727 negative control. Scale bar, 1 μm. (**b**) Gene expression of *ERG10* in *C. albicans* co-
728 cultured with Δ*masH* and *Massilia* sp. YMA for two days revealed by real-time qPCR.
729 Mock represents *C. albicans* growth alone. *C. albicans Act1* was used for internal
730 normalization, and *ERG10* expression levels were further normalized to the Mock
731 condition. The standard error of the mean (SEM) was calculated based on at least
732 three replicates and the Student t-test was used for statistical analysis. ***, $P < 0.001$.
733 (**c**) *C. albicans* are rescued by overexpression of *C. albicans ERG10* from the
734 minimum inhibitory concentration of polyyne treatment (collimonin C/D **1, 2,** and
735 massilin A **3**). The standard deviation was calculated based on three replicates and
736 the Student t-test was used for statistical analysis. ***, $P < 0.001$.

737

References

1. Sanglard D. Emerging Threats in Antifungal-Resistant Fungal Pathogens. *Frontiers in medicine* **3**, 11-11 (2016).

2. Sardi JCO, Scorzoni L, Bernardi T, Fusco-Almeida AM, Mendes Giannini MJS. *Candida* species: current epidemiology, pathogenicity, biofilm formation, natural antifungal products and new therapeutic options. *Journal of medical microbiology* **62**, 10-24 (2013).

3. Pappas PG*, et al.* Clinical Practice Guideline for the Management of Candidiasis: 2016 Update by the Infectious Diseases Society of America. *Clinical infectious diseases : an official publication of the Infectious Diseases Society of America* **62**, e1-50 (2016).

4. Lee Y, Puumala E, Robbins N, Cowen LE. Antifungal Drug Resistance: Molecular Mechanisms in Candida albicans and Beyond. *Chemical Reviews* **121**, 3390-3411 (2021).

5. Yassin MT, Mostafa AA, Al-Askar AA, Bdeer R. In vitro antifungal resistance profile of *Candida* strains isolated from Saudi women suffering from vulvovaginitis. *European Journal of Medical Research* **25**, 1 (2020).

6. Bhattacharya S, Sae-Tia S, Fries BC. Candidiasis and Mechanisms of Antifungal Resistance. *Antibiotics (Basel)* **9**, 312 (2020).

7. Wall G, Lopez-Ribot JL. Current Antimycotics, New Prospects, and Future Approaches to Antifungal Therapy. *Antibiotics (Basel)* **9**, 445 (2020).

8. Negri R. Polyacetylenes from terrestrial plants and fungi: Recent phytochemical and biological advances. *Fitoterapia* **106**, 92-109 (2015).

9. Mullins AJ*, et al.* Genome mining identifies cepacin as a plant-protective metabolite of the biopesticidal bacterium *Burkholderia ambifaria*. *Nat Microbiol* **4**, 996-1005 (2019).

10. W L Parker MLR, V Seiner, W H Trejo, P A Principe, R B Sykes. Cepacin A and cepacin B, two new antibiotics produced by *Pseudomonas cepacia*. *J Antibiot (Tokyo)* **37**, 431-440 (1984).

11. Kai K, Sogame M, Sakurai F, Nasu N, Fujita M. Collimonins A–D, Unstable Polyynes with Antifungal or Pigmentation Activities from the Fungus-Feeding Bacterium *Collimonas fungivorans* Ter331. *Organic Letters* **20**, 3536-3540 (2018).

12. Fritsche K*, et al.* Biosynthetic genes and activity spectrum of antifungal polyynes from *Collimonas fungivorans* Ter331. *Environ Microbiol* **16**, 1334-1345 (2014).

13. M Patel MC, A Horan, D Loebenberg, J Marquez, R Mierzwa, M S Puar, R Yarborough, J A Waitz. Sch 31828, a novel antibiotic from a *Microbispora* sp. taxonomy, fermentation, isolation and biological properties. *J Antibiot (Tokyo)* **41**, 794-797 (1988).

14. Chen PY, Lu N, Lai YM, Yang YL. Anti-microbial metabolites from a marine bacterium YMA4. *Planta Med* **82**, P593 (2016).

15. Kanehisa M, Furumichi M, Tanabe M, Sato Y, Morishima K. KEGG: new perspectives on genomes, pathways, diseases and drugs. *Nucleic Acids Res* **45**, D353-D361 (2017).

16. Blin K, Shaw S, Kautsar SA, Medema MH, Weber T. The antiSMASH database version 3: increased taxonomic coverage and new query features for modular enzymes. *Nucleic Acids Res* **49**, D639-D643 (2021).

17. Hannigan GD*, et al.* A deep learning genome-mining strategy for biosynthetic gene cluster prediction. *Nucleic Acids Research* **47**, e110-e110 (2019).

18. Medema MH, Takano E, Breitling R. Detecting sequence homology at the gene cluster level with MultiGeneBlast. *Mol Biol Evol* **30**, 1218-1223 (2013).

19. Kusumi T, Ohtani I, Nishiyama K, Kakisawa H. Caryoynencins, potent antibiotics from a plant pathogen *Pseudomonas caryophylli*. *Tetrahedron Letters* **28**, 3981-3984 (1987).

20. Ross C, Scherlach K, Kloss F, Hertweck C. The molecular basis of conjugated polyyne biosynthesis in phytopathogenic bacteria. *Angew Chem Int Ed Engl* **53**, 7794-7798 (2014).

21. Murata K, Suenaga M, Kai K. Genome Mining Discovery of Protegenins A–D, Bacterial Polyynes Involved in the Antioomycete and Biocontrol Activities of *Pseudomonas protegens*. *ACS Chemical Biology*, doi.org/10.1021/acschembio.1c00276 (2021).

22. Ueoka R*, et al.* Genome-Based Identification of a Plant-Associated Marine Bacterium as a Rich Natural Product Source. *Angewandte Chemie International Edition* **57**, 14519-14523 (2018).

23. A KR, Shah AH, Prasad R. MFS transporters of *Candida* species and their role in clinical drug resistance. *FEMS Yeast Res* **16**, (2016).

24. Yan Y, Liu N, Tang Y. Recent developments in self-resistance gene directed natural product discovery. *Natural Product Reports* **37**, 879-892 (2020).

25. Hobson C, Chan AN, Wright GD. The Antibiotic Resistome: A Guide for the Discovery of Natural Products as Antimicrobial Agents. *Chem Rev* **121**, 3464-3494 (2021).

26. Chopra I. Over-expression of target genes as a mechanism of antibiotic resistance in bacteria. *The Journal of antimicrobial chemotherapy* **41**, 584-588 (1998).

27. Sutanto F, Konstantinidou M, Domling A. Covalent inhibitors: a rational approach to drug discovery. *RSC Med Chem* **11**, 876-884 (2020).

28. Fan J*, et al.* Tetrameric Acetyl-CoA Acetyltransferase 1 Is Important for Tumor Growth. *Mol Cell* **64**, 859-874 (2016).

29. Ohnuma T, Nakayama S, Anan E, Nishiyama T, Ogura K, Hiratsuka A. Activation of the Nrf2/ARE pathway via S-alkylation of cysteine 151 in the chemopreventive agent-sensor Keap1 protein by falcarindiol, a conjugated diacetylene compound. *Toxicol Appl Pharmacol* **244**, 27-36 (2010).

30. Modis Y, Wierenga RK. A biosynthetic thiolase in complex with a reaction intermediate: the crystal structure provides new insights into the catalytic mechanism. *Structure* **7**, 1279-1290 (1999).

31. Kim S*, et al.* Redox-switch regulatory mechanism of thiolase from *Clostridium acetobutylicum*. *Nat Commun* **6**, 8410 (2015).

32. Zhang Y, Wei W, Fan J, Jin C, Lu L, Fang W. *Aspergillus fumigatus* Mitochondrial Acetyl Coenzyme A Acetyltransferase as an Antifungal Target. *Appl Environ Microbiol* **86**, (2020).

33. Haapalainen AM, Meriläinen G, Pirilä PL, Kondo N, Fukao T, Wierenga RK. Crystallographic and Kinetic Studies of Human Mitochondrial Acetoacetyl-CoA Thiolase: The Importance of Potassium and Chloride Ions for Its Structure and Function. *Biochemistry* **46**, 4305-4321 (2007).

34. Modis Y, Wierenga RK. A biosynthetic thiolase in complex with a reaction intermediate: the crystal structure provides new insights into the catalytic mechanism. *Structure* **7**, 1279-1290 (1999).

35. Lewis K. Platforms for antibiotic discovery. *Nat Rev Drug Discov* **12**, 371-387 (2013).

36. Chen A, Re RN, Burkart MD. Type II fatty acid and polyketide synthases: deciphering protein-protein and protein-substrate interactions. *Nat Prod Rep* **35**, 1029-1045 (2018).

37. Soucy SM, Huang J, Gogarten JP. Horizontal gene transfer: building the web of life. *Nat Rev Genet* **16**, 472-482 (2015).

38. Palmer AC, Kishony R. Opposing effects of target overexpression reveal drug mechanisms. *Nature Communications* **5**, 4296 (2014).

875 39. Sugden CJ, Roper JR, Williams JG. Engineered gene over-expression as a method of
876 drug target identification. *Biochemical and Biophysical Research Communications*
877 **334**, 555-560 (2005).
878
879 40. Saraon P*, et al.* Evaluation and prognostic significance of ACAT1 as a marker of
880 prostate cancer progression. *Prostate* **74**, 372-380 (2014).
881
882 41. Jiang P*, et al.* In vitro and in vivo anticancer effects of mevalonate pathway
883 modulation on human cancer cells. *Br J Cancer* **111**, 1562-1571 (2014).
884
885 42. Bloxham DP, Chalkley RA, Coghlin SJ, Salam W. Synthesis of chloromethyl ketone
886 derivatives of fatty acids. Their use as specific inhibitors of acetoacetyl-coenzyme A
887 thiolase, cholesterol biosynthesis and fatty acid synthesis. *Biochemical Journal* **175**,
888 999-1011 (1978).
889
890 43. Holland PC, Clark MG, Bloxham DP. Inactivation of pig heart thiolase by 3-butynoyl
891 coenzyme A, 3-pentynoyl coenzyme A, and 4-bromocrotonyl coenzyme A.
892 *Biochemistry* **12**, 3309-3315 (1973).
893
894 44. Palmer MA*, et al.* Biosynthetic thiolase from *Zoogloea ramigera*. Evidence for a
895 mechanism involving Cys-378 as the active site base. *The Journal of biological*
896 *chemistry* **266**, 8369-8375 (1991).
897
898 45. Kumar S, Stecher G, Li M, Knyaz C, Tamura K. MEGA X: Molecular Evolutionary
899 Genetics Analysis across Computing Platforms. *Molecular biology and evolution* **35**,
900 1547-1549 (2018).
901
902 46. Letunic I, Bork P. Interactive Tree Of Life (iTOL) v4: recent updates and new
903 developments. *Nucleic Acids Research* **47**, W256-W259 (2019).
904
905 47. Shevchenko A, Tomas H, Havlis J, Olsen JV, Mann M. In-gel digestion for mass
906 spectrometric characterization of proteins and proteomes. *Nat Protoc* **1**, 2856-2860
907 (2006).
908
909 48. Diament BJ, Noble WS. Faster SEQUEST searching for peptide identification from
910 tandem mass spectra. *J Proteome Res* **10**, 3871-3879 (2011).
911
912 49. Long T, Sun Y, Hassan A, Qi X, Li X. Structure of nevanimibe-bound tetrameric human
913 ACAT1. *Nature* **581**, 339-343 (2020).
914
915 50. Otwinowski Z, Minor W. Processing of X-ray diffraction data collected in oscillation
916 mode. *Methods in enzymology* **276**, 307-326 (1997).
917
918 51. Kantardjieff KA, Rupp B. Matthews coefficient probabilities: Improved estimates for
919 unit cell contents of proteins, DNA, and protein–nucleic acid complex crystals.
920 *Protein Science* **12**, 1865-1871 (2003).
921

52. Vagin A, Teplyakov A. Molecular replacement with MOLREP. *Acta crystallographica Section D, Biological crystallography* **66**, 22-25 (2010).

53. Cowtan K. The Buccaneer software for automated model building. 1. Tracing protein chains. *Acta crystallographica Section D, Biological crystallography* **62**, 1002-1011 (2006).

54. Perrakis A, Morris R, Lamzin VS. Automated protein model building combined with iterative structure refinement. *Nature structural biology* **6**, 458-463 (1999).

55. Emsley P, Cowtan K. Coot: model-building tools for molecular graphics. *Acta crystallographica Section D, Biological crystallography* **60**, 2126-2132 (2004).

56. Murshudov GN*, et al.* REFMAC5 for the refinement of macromolecular crystal structures. *Acta Crystallographica Section D* **67**, 355-367 (2011).

57. Williams CJ*, et al.* MolProbity: More and better reference data for improved all-atom structure validation. *Protein science : a publication of the Protein Society* **27**, 293-315 (2018).

58. Lambert RJW, Pearson J. Susceptibility testing: accurate and reproducible minimum inhibitory concentration (MIC) and non-inhibitory concentration (NIC) values. *Journal of Applied Microbiology* **88**, 784-790 (2000).